LBL-21867

Modeling of Porous Electrodes in Molten-Salt Systems†

John Newman

Materials and Molecular Research Division,
Lawrence Berkeley Laboratory, and
Department of Chemical Engineering,
University of California, Berkeley

August 9, 1986

Abstract

Porous electrodes are used for many batteries because they permit the reactants to be close to the site of the electrochemical reaction. The basis for a nonuniform reaction distribution in such electrodes is reviewed, and some results are discussed for lithium alloy, iron sulfide cells. Discrepancies between model and experimental results can be attributed to poor approximations to the effective conductivity of packed-bed electrodes and to inadequate treatment of the precipitation of KCl.

†Presented at the International Workshop on High-Temperature Molten Salt Batteries, Argonne National Laboratory, April 16-18, 1986.

Here we want to go over, by way of background, some of the fundamentals of porous-electrode theory and expected behavior. This will be further illustrated by the modeling of molten-salt cells, including some problems and possibilities for improvement.

Figure 1 illustrates the concept of a porous electrode, in which reactants are embedded in an electronically conducting matrix which is permeated by an electrolyte. In this example, current enters the electrode through an electronic current from the left into the matrix. Somewhere within the volume of the porous electode, an electrochemical reaction occurs, and the current emerges at the right as ionic current within the electrolyte. An obvious advantage of porous electrodes is the high interfacial area, which can minimize the surface overpotential associated with the electrochemical reaction. A second major advantage for battery applications is the possibility to store reactants close to the reaction site. These can include insoluble reactants, such as iron sulfide, soluble reactants, such as sulfuric acid in a lead-acid cell, or gaseous reactants, such as in fuel cells. Porous electrodes find uses in primary and secondary batteries, flow redox energy storage systems, and in flow-through electordes for metal ion removal by plating or ion adsorption.

The modeling of porous electrodes involves establishing a number of unknowns which one needs to determine and a set of governing equations. In this application, these equations are likely to include transport processes, such as Ohm's law in the matrix and the description of migration, diffusion, and convection in the solution, material balances on liquid and solid phases, and reaction kinetics for electrochemical reactions. The distributed resistor network in Figure 2 illustrates why the reaction is

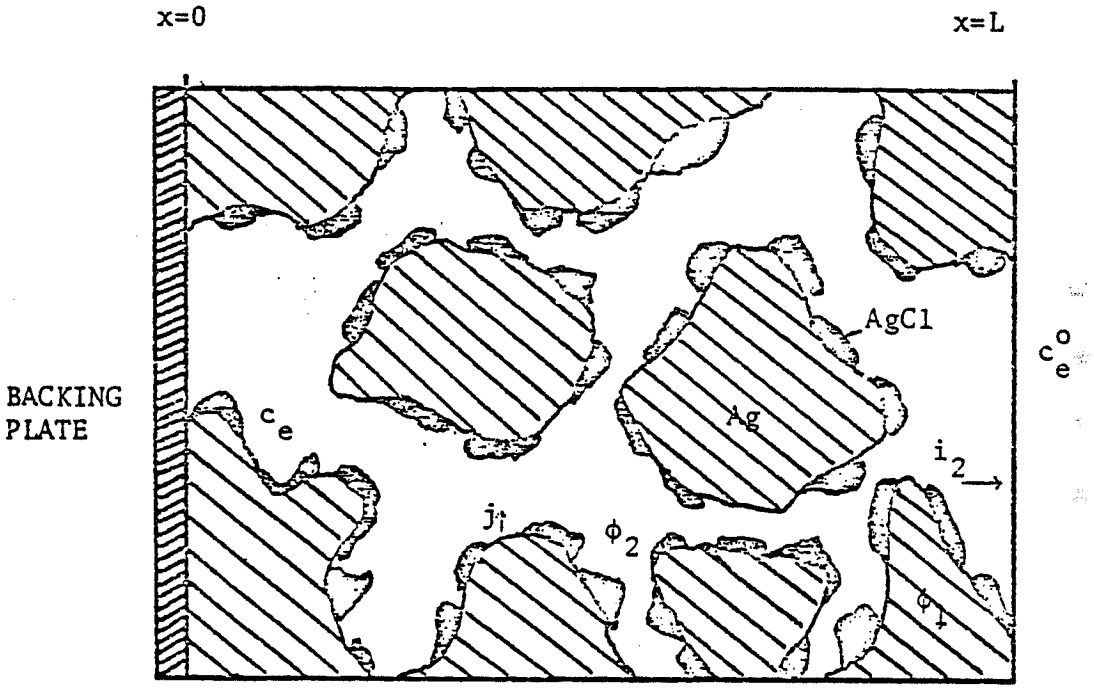

Figure 1. Schematic of a porous electrode, showing solution and matrix phases and a solid reactant. The current collector is at the left, and the separator and counterelectrode are at the right.

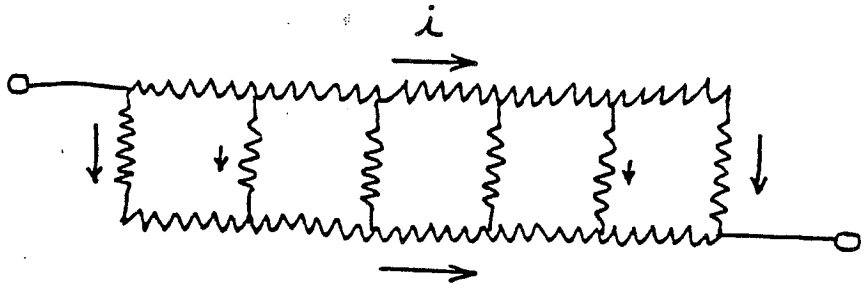

Figure 2. Resistor network illustrating the mechanism of the distribution of current in a porous electrode.

nonuniform and distributed throughout the volume of the porous electrode. The circle at the left can represent the current collector, and the upper resistor series the electronically conducting matrix. The circle at the right can represent the separator, and the lower resistor series the ionically conducting pore solution. The vertical resistors represent the electrochemical reaction whereby charge is transferred from the matrix to the solution. Charge flowing from left to right must react within the network, and it will try to distribute itself between the matrix and the solution (that is, between the upper and the lower resistor series) in inverse relation to their resistivities. Thus, the reaction has a tendency to occur near the left or the right and to be relatively absent within the middle of the electrode. If the resistance of the electrochemical reaction is high, the distribution will tend to be uniform. A low resistivity for the matrix phase tends to shift the reaction towards the right, towards the separator.

Figure 3 shows the cell sandwich which represents a molten-salt cell designed to form part of a high-power battery. The current that we had been following in the single-electrode system now continues through the separator and into the positive electrode where a cathodic reaction results in the current flow now being in the electonically conducting matrix and thence to the positive current collector. Electrode reactions are indicated for a negative made of LiAl and for one of the reactions of an iron sulfide positive. At the temperatures of molten salts, the electrode kinetics tend to be relatively fast. As an alternative to the reaction of FeS to Li_2FeS_2 (also called "*X*" phase), the reaction can go through a complex compound called "*J*" phase (which is $LiK_6Fe_{24}S_{26}Cl$) according to the following scheme:

$$26\ FeS + Li^+ + Cl^- + 6\ K^+ + 6\ e^- \rightarrow LiK_6Fe_{24}S_{26}Cl + 2\ Fe$$

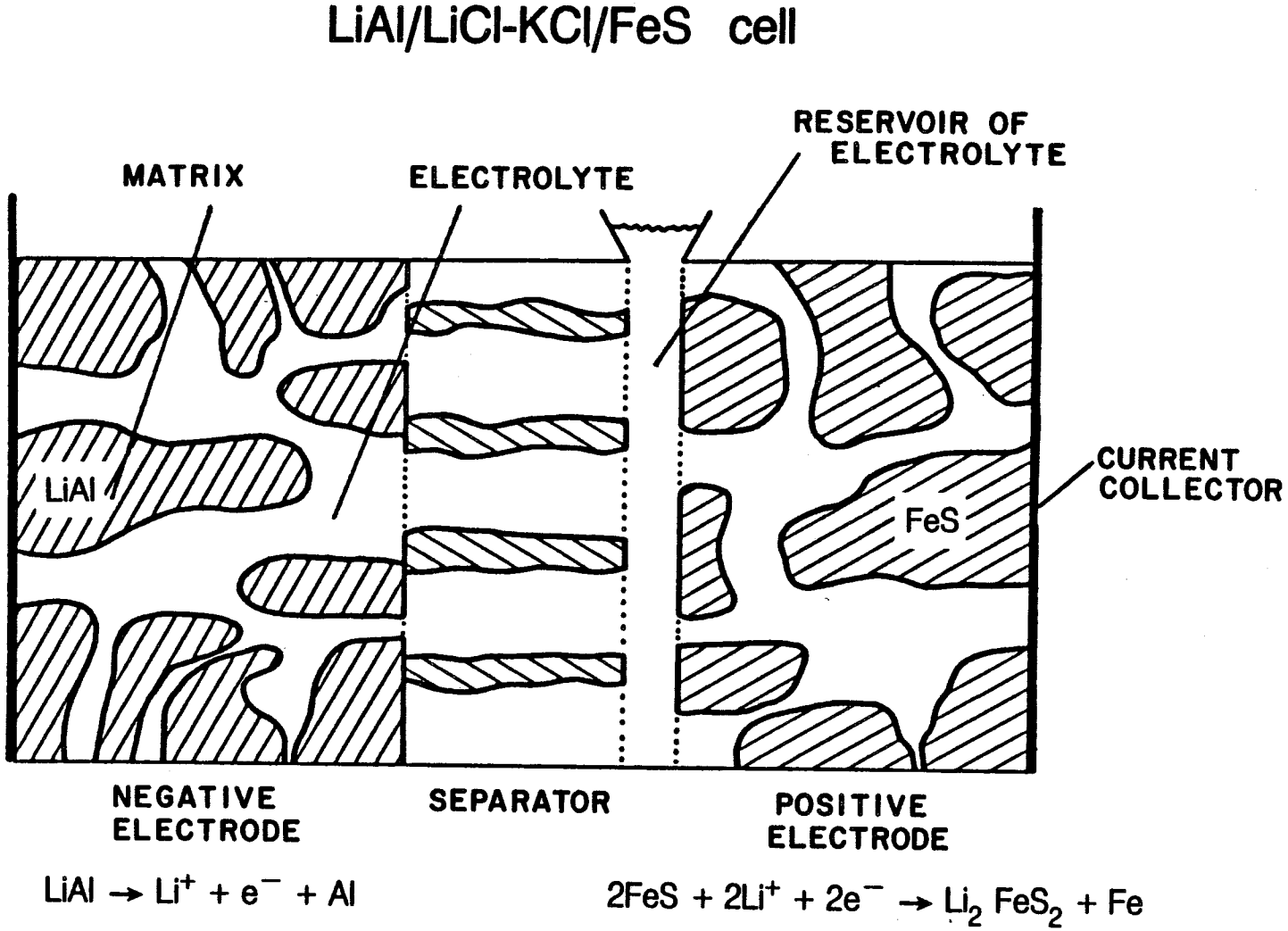

Figure 3. Schematic diagram of the LiAl/FeS cell.

followed by the reaction of J phase to other compounds, such as

$$J + 25\ Li^+ + 20\ e^- \rightarrow 13\ Li_2FeS_2 + 11\ Fe + 6\ K^+ + Cl^-.$$

Figure 4 shows concentration profiles for a LiAl/FeS cell discharging through the Li_2FeS_2 ("X" phase) mechanism. At short times, the concentration profiles reflect the stoichiometry of the electrode reactions. In the negative, Li^+ ions are injected into the electrolyte, thus raising the mole fraction of LiCl, while in the positive, Li^+ ions are extracted from the melt, thus lowering the mole fraction of LiCl. The figure shows that the reactions occur relatively close to the separator, since the locations of injection and extraction occur close to the separator, and one can see the regions moving into the depth of the electrodes as time progresses. The negative electrode is opening up as the reaction occurs, and the concentration profiles are not very sharp there, while in the positive electrode, the porosity is small after the first reaction, and the progress of the reaction front through the electrode is clearly visible. The reaction front is also less distinct in the negative electrode because this is an alloy electrode, and changes in the composition of the LiAl alloy result in concentration overpotentials which tend to spread out the reaction region over the depth of the electrode. After 2.5 hours, a second reaction front is visible in the positive, before the first reaction front has reached the back of the electrode. The second reaction (of Li_2FeS_2 to Fe and Li_2S) also produces an even smaller porosity, and concentration gradients become even more pronounced in the positive. This eventually leads to precipitation of KCl in the positive, and in the model this causes the cell potential to drop drastically if the precipitate blocks the pore cross-section.

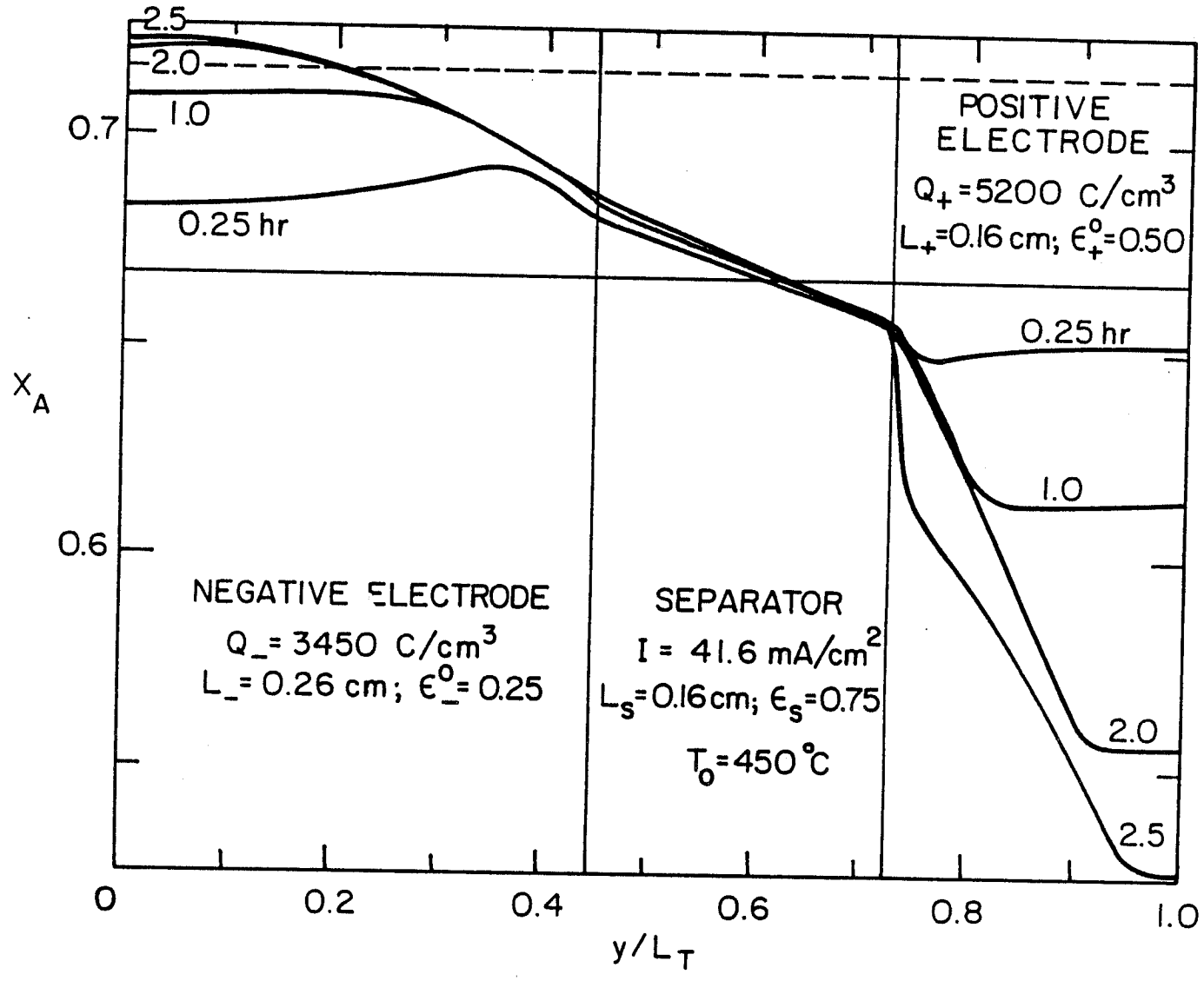

Figure 4. Position dependence of mole fraction of LiCl at different discharge times. Dashed line represents saturation limit for LiCl at 450°C.

Figure 5 shows contrasting concentration profiles predicted for the reaction through the J phase. Here the mole fraction rises in the positive as well as the negative in the early stages of discharge because K^+ ions are extracted in greater numbers than Li^+ ions. However, the following reaction in the positive brings the mole fraction down again, and more drastically than in the X phase mechanism, because no Li^+ ions were transferred during the early stages of the discharge.

Figure 6 shows predicted discharge curves (for the X-phase mechanism) contrasted with experimental cell-potential data. The model results follow the experimental results reasonably well in the latter part of the discharge if precipitation of KCl is precluded in the model. The curves labeled A and B indicate the early termination of the discharge if precipitation is allowed to occur.

Figure 7 shows predicted and experimental results for the discharge of a $LiAl/FeS_2$ cell. The top curve (with several line segments) corresponds to a reversible discharge and is based on thermodynamic cell potentials. The model calculations lie slightly below the reversible curve, and the experimental results lie below that. All three curves reflect the reaction sequence believed to apply to the FeS_2 electrode. In the early stages of discharge, the model results do not show as much polarization as the experimental curve, indicating that resistances within the electrodes are not properly accounted for. Also, the model results show an end of discharge, due to precipitation, much earlier than the experimental curve. This illustrates the two major discrepancies between the model and the experiment: there is too little voltage loss and too much precipitation.

Figure 8 shows volume fractions of various phases at a point in the discharge of the FeS electrode by means of the X-phase mechanism. Here both reaction fronts can

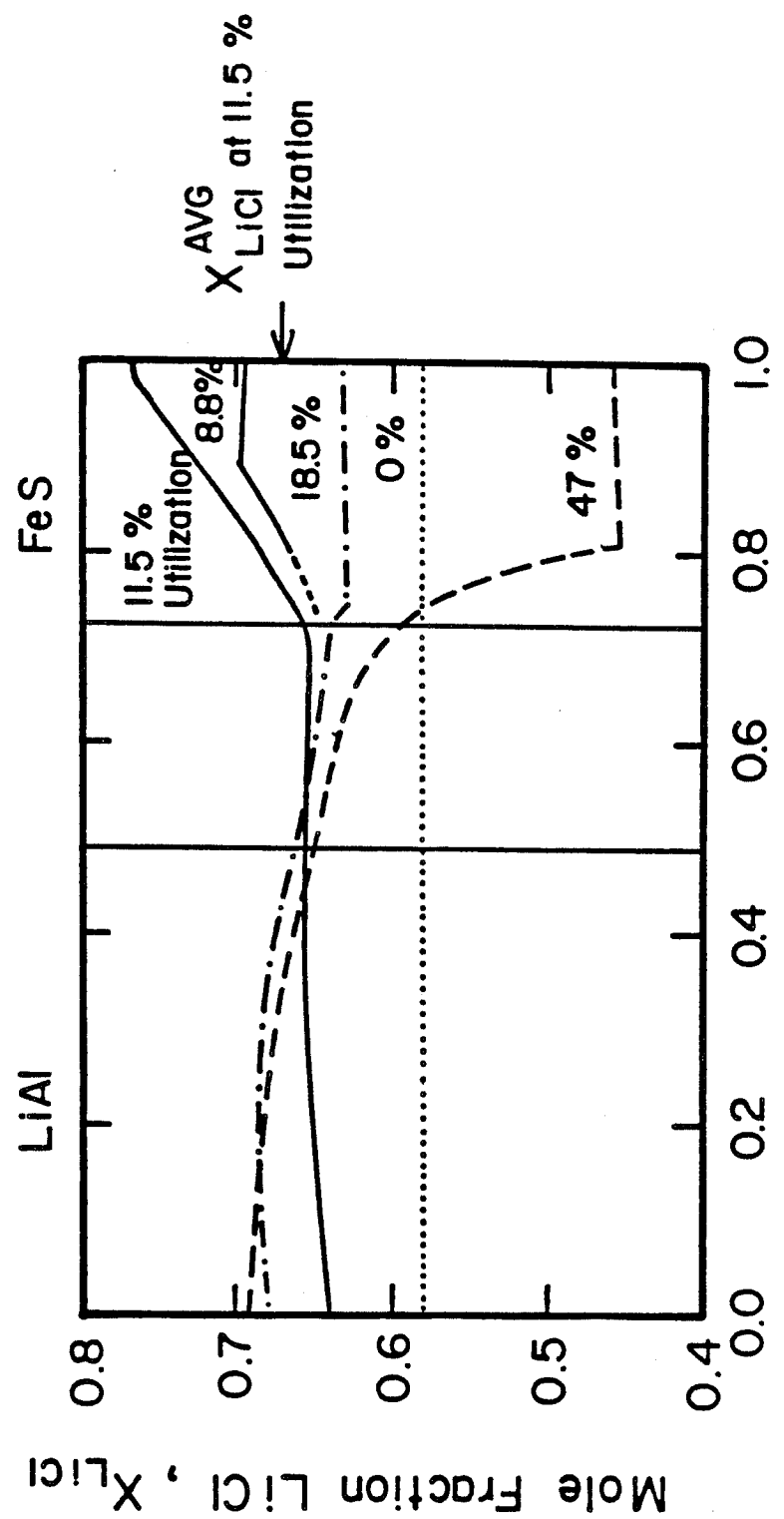

Figure 5. Position dependence of the mole fraction of LiCl at different states of discharge for the *J*-phase mechanism.

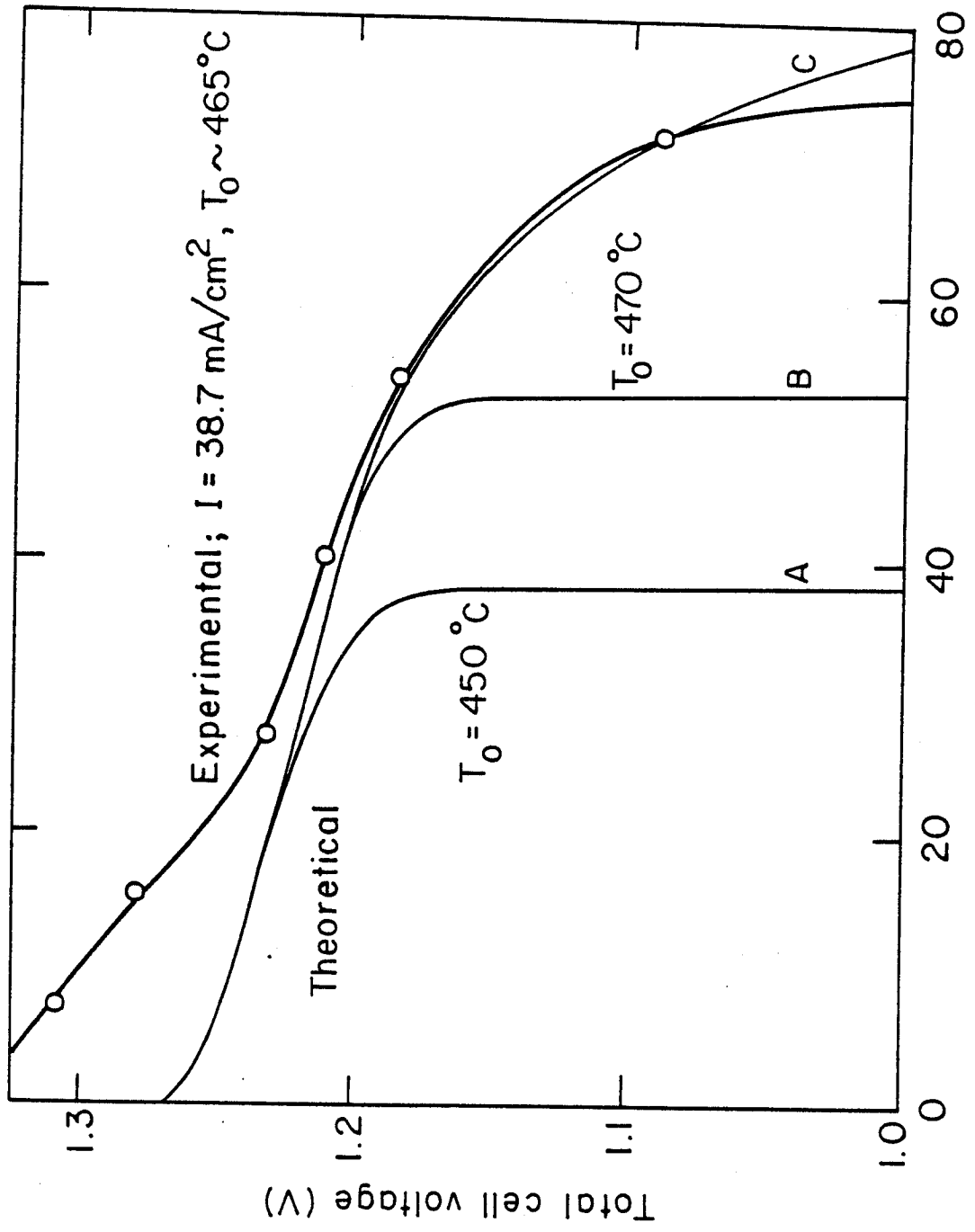

Figure 6. Comparison of theoretical and experimental discharge curves for the X-phase mechanism.

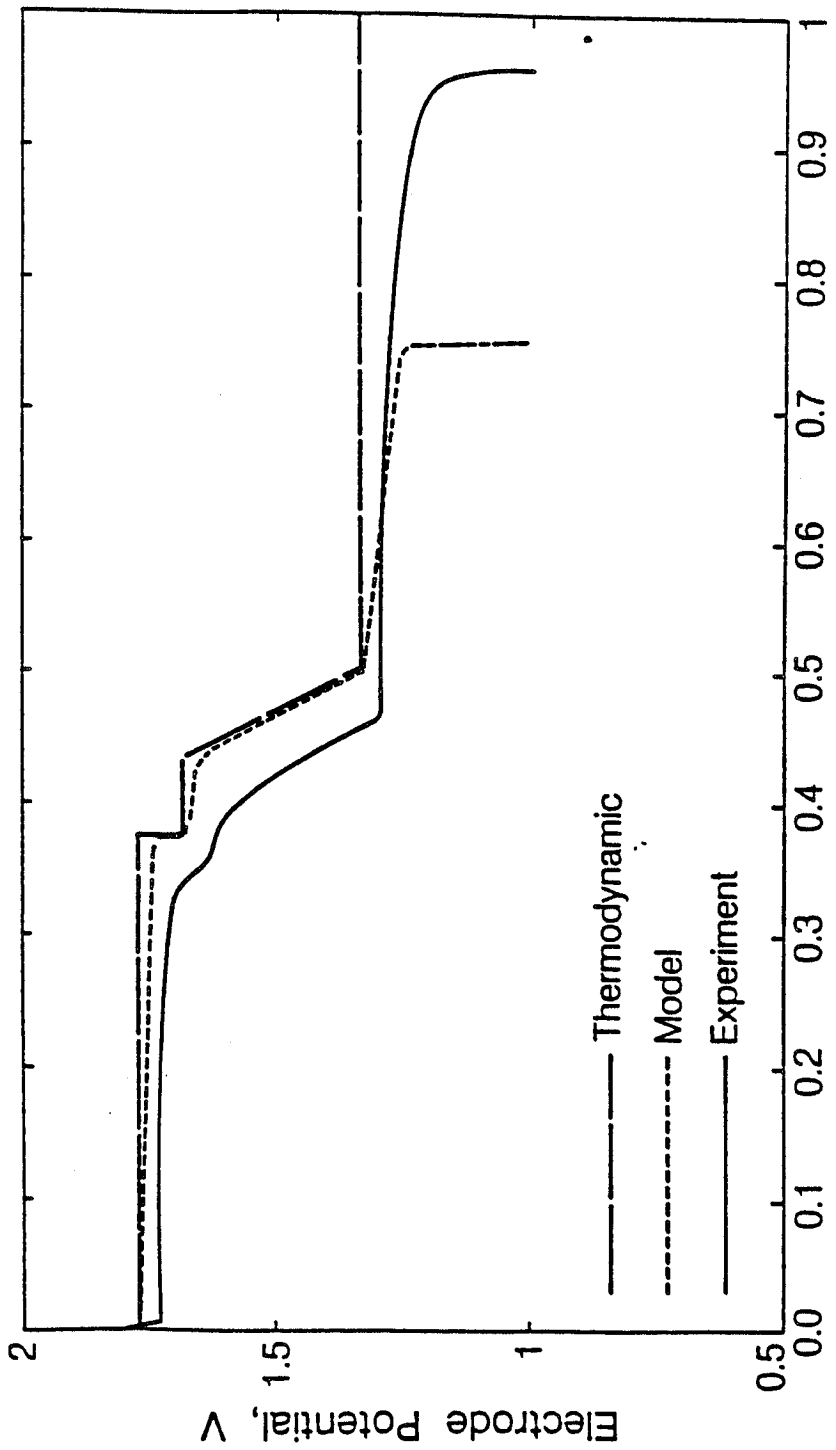

Figure 7. Comparison of model and experimental results for the voltage of the FeS_2 electrode in a LiAl/FeS_2 cell, relative to a LiAl (α–β) reference electrode (450°C, 50 mA/cm^2, x^0_{LiCl} = 0.68). The reversible, thermodynamic potential is also shown in order to display more clearly the losses of the system.

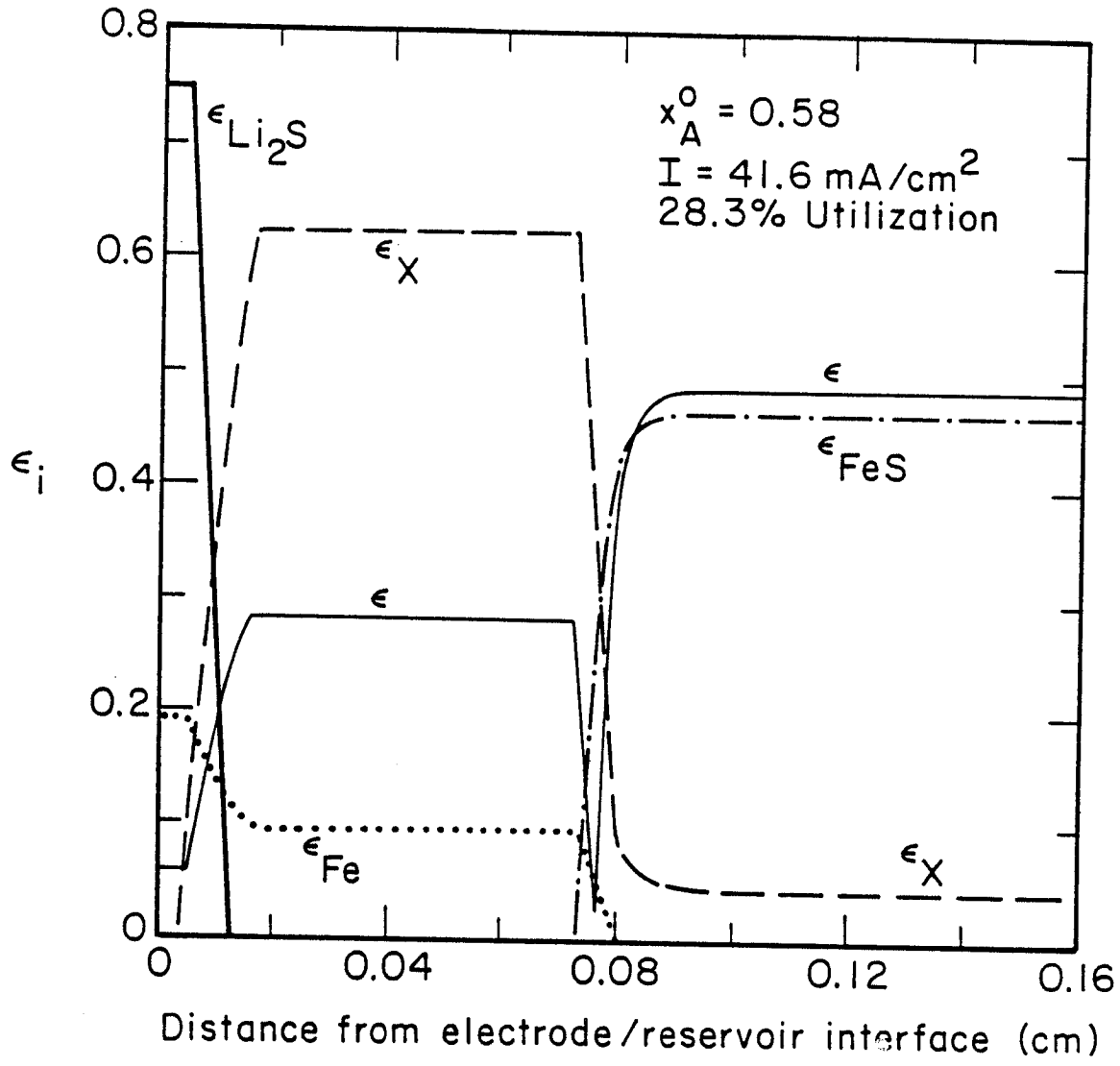

Figure 8. Volume fractions of solid phases and electrolyte in the positive electrode of a LiAl/FeS cell discharging by the X-phase mechanism.

be seen; the front for the first reaction is at about 0.077 cm, and that for the second reaction is at about 0.01 cm. The initial porosity is about 0.5, and this is reduced to about 0.29 after the first reaction and to about 0.06 after the second reaction. However, at the reaction front for the first reaction, the porosity drops sharply to a small value over a very small distance. This is due to the calculated precipitation of KCl in the positive electrode, and this causes the discharge potential to drop considerably, eventually leading to the prediction of the end of discharge.

There are several things that one can try in order to improve the agreement with experiment and to enhance our understanding of the discharge process in these systems:

1. Improve the representation of the conductivity of composite solids, such as form the positive electrode of these cells.

2. Try to account for the swelling of the positive electrode on discharge.

3. Investigate whether convection could produce better mixing and thus delay precipitation of KCl.

Figure 9 shows the observed swelling of the positive electrode during cycling, as a percent above its constructed thickness. At the right one sees that the electrode is expanded beyond the fabrication thickness even at full charge. This is taken into account in the model because the thicknesses of the electrodes and the separator are chosen to represent the values after the cell has gone through several "break-in" cycles. The positive electrode expands during discharge, exerting pressure on the separator and thence on the negative, so that the negative and the separator decrease in thickness during discharge. This behavior will tend to discourage precipitation of KCl in the positive.

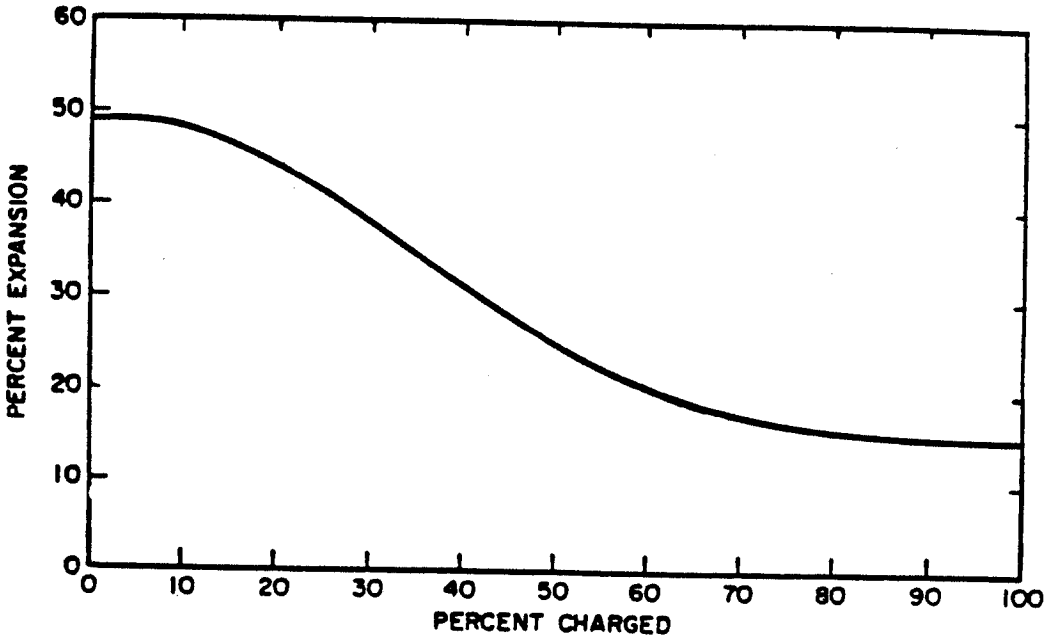

Figure 9. Average positive-electrode expansion of a series of experimental cells as a function of state of charge.

In order to get an idea of the magnitude of this effect, we have run the FeS model with several, constant values of the positive-electrode porosity and have recorded the predicted utilization of the electrode, before precipitation terminates the discharge. We have translated these different initial porosites into amounts of electrode expansion and represented the results in Figure 10. These results are for the *J*-phase mechanism. One can infer the additional capacity that might be predicted with expansion amounts corresponding to the end of discharge (where the precipitation problem is most acute) and to the middle of discharge.

In summary, let us emphasize that models of batteries with porous electrodes can predict polarization characteristics, as well as temperature changes. They can also give details of the what is going on inside, such as composition profiles, precipitation of electrolyte, and reaction and porosity distributions, which would be difficult to determine experimentally. These details, as well as attempts to reconcile results with experiments, can enhance our understanding of how such systems operate.

Acknowledgment

This work was supported by the Assistant Secretary of Conservation and Renewable Energy, Office of Energy Systems Research, Energy Storage Division of the United States Department of Energy under Contract Number DE-AC03-76SF00098.

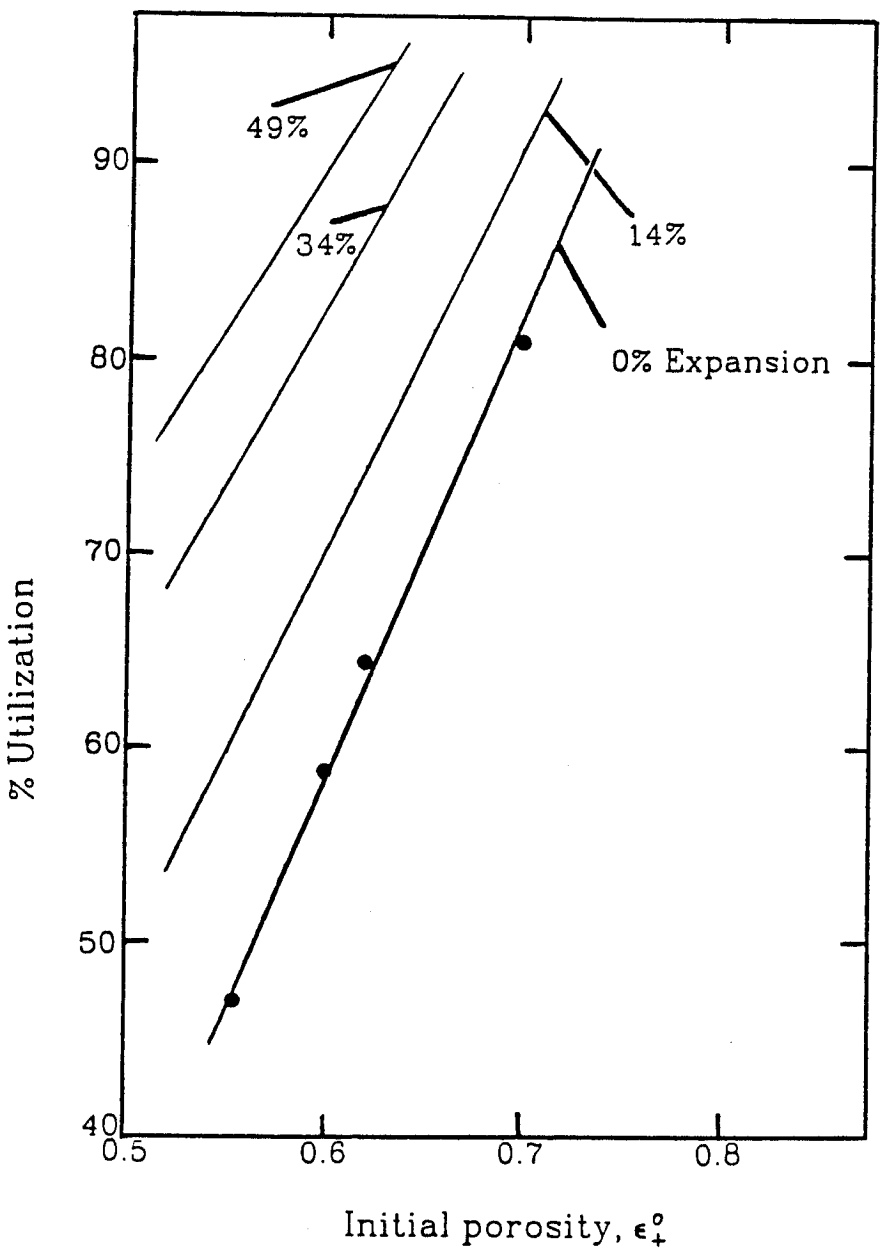

Figure 10. Maximum positive electrode utilization as a function of ϵ_+^0. The points are simulation results.